We are IntechOpen,
the world's leading publisher of Open Access books
Built by scientists, for scientists

6,900
Open access books available

185,000
International authors and editors

200M
Downloads

154
Countries delivered to

Our authors are among the

TOP 1%
most cited scientists

12.2%
Contributors from top 500 universities

CLARIVATE ANALYTICS
BOOK CITATION INDEX
INDEXED

WEB OF SCIENCE™

Selection of our books indexed in the Book Citation Index
in Web of Science™ Core Collection (BKCI)

Interested in publishing with us?
Contact book.department@intechopen.com

Numbers displayed above are based on latest data collected.
For more information visit www.intechopen.com

8

Differential Absorption Microwave Radar Measurements for Remote Sensing of Barometric Pressure

Roland Lawrence[1], Bin Lin[2], Steve Harrah[2] and Qilong Min[3]
[1]Old Dominion University
[2]NASA Langley Research Center
[3]SUNY at Albany
USA

1. Introduction

1.1 Overview

As coastal regions around the world continue to grow and develop, the threat to these communities from tropical cyclones also increases. The predicted sea level rise over the next decades will certainly add to these risks. Developed low-lying coastal regions are already of major concern to emergency management professionals. While hurricane forecasting is available, improved predictions of storm intensity and track are needed to allow the time to prepare and evacuate larger cities. The predictions and forecasts of the intensity and track of tropical storms by regional numerical weather models can be improved with the addition of large spatial coverage and frequent sampling of sea surface barometry. These data are critically needed for use in models.

This chapter will present recent advances in the development of a microwave radar instrument technique to remotely sense barometric pressure over the ocean and may provide the large-scale sea surface barometric pressure data needed to substantially improve the tropical storm forecasts. The chapter will include a brief introduction, a discussion of the applications of remote sensing of sea surface barometric pressure, a discussion of the theoretical basis for the differential absorption radar concept, the results of laboratory and flight testing using a prototype radar, and a detailed discussion of the performance challenges and requirements of an operational instrument.

1.2 Background

Surface air pressure is one of the most important atmospheric parameters that are regularly measured at ground based surface meteorological stations. Over oceans, sea surface air barometric pressures are usually measured by limited numbers of in-situ observations conducted by buoy stations and oil platforms. The spatial coverage of the observations of this dynamically critical parameter for use by weather forecasters is very poor. For example, along the east coast of the United States and Gulf of Mexico, only about 40 buoys are

available under the NOAA Ocean Observing System (NOOS) of the NOAA National Data Buoy Center (NDBC; http://www.ndbc.noaa.gov/). The tropical atmosphere ocean (TAO) program only has 10 sites from which the barometric pressure is measured. For severe weather conditions, such as tropical storms and hurricanes, these NOOS and TAO buoy systems usually cannot provide spatially desirable in-situ measurements due to either the lack of buoy stations along the actual track of the storm or malfunctions of buoys caused by the severe weather itself.

Under tropical cyclone conditions, including tropical depression, tropical storm, hurricane, and super-typhoon cases, the surface barometric pressure is one of the most important meteorological parameters in the prediction and forecast of the intensity and track of tropical storms and hurricanes. The central air pressure at sea level of tropical cyclones is the most commonly used indicator for hurricane intensity. The classification of tropical storms and hurricanes on the Saffir-Simpson Hurricane Scale (SSHS) is based on the maximum sustained surface wind speed that is a direct result of the interaction between the central air pressure and the pressure fields surrounding tropical storms. Because intensity predictions and landfall forecasts heavily rely upon them, measurements of the central pressure of tropical storms are extremely important. The only method currently available for use is a manned aircraft dropsonde technique. The problem with the dropsonde technique is that each dropsonde supplies only one spatial point measurement at one instant of interest during the passage of the storm. This limits data to the number of dropsondes used and their spatial distribution and thereby leaves most of the storm area unmeasured. Furthermore, dropsondes are difficult to precisely position and cannot be reused. Figure 1 shows the current capability for sea surface barometric measurements; all of them are in situ observations.

To improve predictions and forecasts of the intensity and track of tropical storms, large spatial coverage and frequent sampling of sea surface barometry are critically needed for use in numerical weather models. These needed measurements of sea surface barometric pressure cannot be realized by in-situ buoy and aircraft dropsonde techniques. One approach that may provide barometry in large spatial and temporal scales over oceans is the use of remote sensing techniques including those on board manned aircraft, unmanned aerial vehicles (UAVs), and satellite platforms.

During the last two decades, the development of remote sensing methods, especially airborne and satellite techniques, for large and global scale sea surface pressure measurements significantly lagged methods for other important meteorological parameters,

Fig. 1. Drift Buoy (left), Moored Buoy (middle), and Dropsonde (right).

such as temperature and humidity. There have been suggestions for using satellite oxygen A-band methods, both passive and active, to measure pressure (Barton & Scott, 1986; Korb & Weng, 1982; Singer, 1968; Wu, 1985; and references therein). The active instruments rely on the operation of complicated, highly-stable laser systems on a space platform and are thus technically difficult. Passive methods are restricted to daytime measurements and areas of low cloud cover (Barton & Scott, 1986). Although substantial research efforts have been underway, there are no realizations of remote sensing measurements for atmospheric surface pressure presently available.

This chapter will describe the development of an active microwave radar working at moderate to strong O_2 absorption bands in the frequency range of 50~56 GHz for surface barometric pressure remote sensing, especially over oceans. The sensor concept and flight testing of a proof-of-concept O_2-band radar system for sea surface air pressure remote sensing will also be discussed. At these radar wavelengths, the reflection of radar echoes from water surfaces is strongly attenuated by atmospheric column O_2 amounts. Because of the uniform mixture of O_2 gases within the atmosphere, the atmospheric column O_2 amounts are proportional to atmospheric path lengths and atmospheric column air amounts, thus, to surface barometric pressures. Historically, (Flower & Peckham, 1978) studied the possibility of a microwave pressure sounder using active microwave techniques. A total of six channels covering frequencies from ~25GHz to ~75GHz were considered. A major challenge in this approach is the wide spectral region and the significant additional dependence of radar signals on microwave absorption from liquid water (LW) clouds and atmospheric water vapor (WV) over this range of frequencies. Atmospheric and cloud water temperatures also have different effects on the absorptions at different wavelengths (Lin et al., 1998a, 1998b, 2001). The complexity in matching footprints and obtaining accurate surface reflectivities of the six different wavelength channels makes their system problematic (Barton & Scott, 1986). Recently, (Lin & Hu, 2005) have considered a different technique that uses a dual-frequency, O_2-band radar to overcome the technical obstacles. They have outlined the characteristics of the novel radar system, and simulated the system performance. The technique uses dual wavelength channels with similar water vapor and liquid water absorption characteristics, as well as similar footprints and sea surface reflectivities, because of the closely spaced spectra. The microwave absorption effects due to LW and WV and the influences of sea surface reflection should be effectively removed by use of the ratio of reflected radar signals of the two channels. Simulated results (Lin & Hu, 2005) suggest that the accuracy of instantaneous surface air pressure estimations from the echo ratio could reach 4 – 7 millibars (mb). With multiple pressure measurements over less than ~1km² sea surface spots from the radar echoes, the pressure estimates could be significantly reduced to a few millibars, which is close to the accuracy of in situ measurements and very useful for tropical storm and large scale operational weather modeling and forecasting over oceans.

2. Sea surface barometric pressure measurements for hurricane forecasts

One of the proposed applications of the Differential Absorption Barometric Radar, hereafter called DiBAR, is to improve weather forecasts and predictions, especially for tropical storms. To address the usefulness of sea surface barometric measurements from DiBAR, we use weather prediction models to simulate predicted hurricane intensities and tracks. Predicted results with sea surface air pressure data incorporated are compared with those

without the pressure measurements. These surface pressures were obtained from later analysis of in-situ measurements and the assimilated data of the actual hurricane events. During these actual hurricane events, these sea surface pressure data were not available a priori for modeling and prediction. Quantitative potential improvements in the forecasts and predictions of studied hurricane cases are evaluated. We emphasize that the sea surface air pressure data injected into weather prediction models are not exactly the same as those from later analysis of in-situ measurements and the assimilated data of the actual hurricane events. Some uncertainties exist in the injected pressure data in our simulations to reflect potential DiBAR remote sensing errors, according to our current understanding of DiBAR systems and retrieval uncertainties. This section provides a brief description of the weather forecast model used to simulate the impact of pressure data consistent with our instrument concept, as well as, the results of our study to simulate the improved track and intensity predictions that result from the inclusion of the simulated DiBAR pressure data.

2.1 Weather forecast model description

The numerical weather forecast model used in this study is the Advanced Regional Prediction System (ARPS) developed by the Center for Analysis and Prediction of Storms (CAPS) of the University of Oklahoma and adopted by NASA Langley Research Center (Wang et al., 2001; Xue et al., 2003; Wang & Minnis, 2003). The forward prediction component of the ARPS is a three-dimensional, non-hydrostatic compressible model in a terrain-following coordinate system. The model includes a set of equations for momentum, continuity, potential temperature, water vapor, and turbulence kinetic energy (TKE). It also includes five conservation equations for hydrometeor species: cloud water (small cloud liquid droplets), cloud ice (small ice crystals), rain, snow, and hail (Tao & Simpson 1993). The cloud water and cloud ice move with the air, whereas the rain, snow, and hail fall with their terminal velocity. It has multiple-nested capability to cover the cloud-scale domain and mesoscale domain at the same time. The model employs advanced numerical techniques (e.g., a flux-corrected transport advection scheme, a positive definite advection scheme, and the split-time step). The most unique physical processes included in the model system are a scheme of Kessler-type warm-rain formation and 3-type ice (ice, snow, and hail) microphysics; a soil-vegetation land-surface model; a 1.5-order TKE-based non-local planetary boundary layer parameterization scheme; a cloud-radiation interaction atmospheric radiative transfer scheme; and some cumulus parameterization schemes used for coarse grid-size. Furthermore, a sophisticated long- and short-wave cloud-radiation interaction package (Chou, 1990, 1992; Chou & Suarez, 1994) has been applied to the ARPS model. The ARPS can provide more physically realistic 4D cloud information in very-high-resolution of spatial (cloud processes) and temporal (minutes) scales (Figure. 2).

The ARPS model was run in a horizontal domain of 4800 km, east-west and 4000 km, south-north, and a vertical domain of 25 km. The horizontal grid spacing is 25 km, and the vertical grid space varies from 20 m at the surface to 980 m at the model top. These spatial resolutions are used because they are comparable to those of the models used in the Global Modeling and Assimilation Office, NASA Goddard Space Flight Center. The options for ice microphysics and atmospheric cloud-radiation interactive transfer parameterization were both used in the model. Because of the use of the relatively coarser grid-size of 25 km, the new Kain & Fritsch cumulus parameterization scheme was used together with explicit ice microphysics.
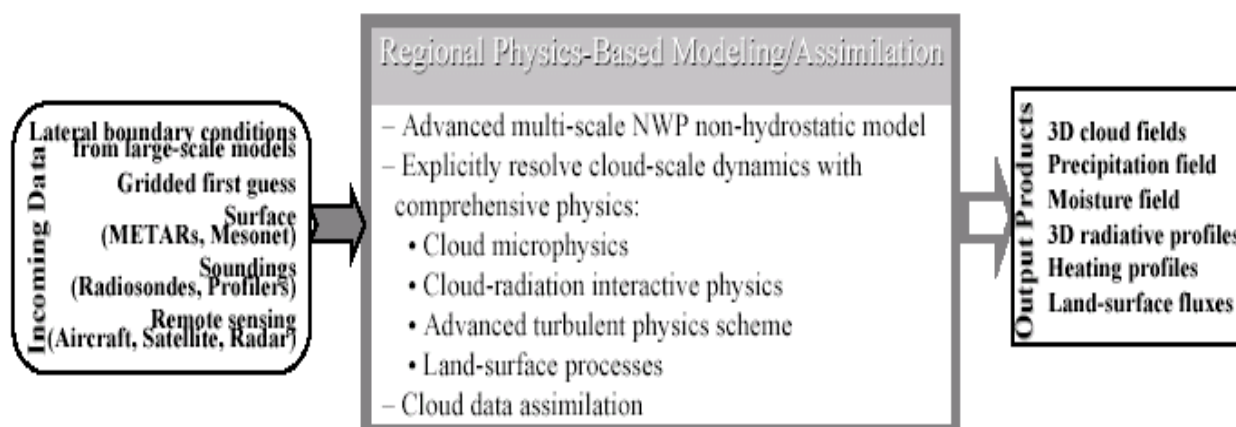
Fig. 2. ARPS: a regional cloud-scale modeling/assimilation system.

2.2 Forecast improvements with the addition of storm central pressure measurements

The analyzed case here is hurricane Ivan (2004). Ivan was a classical, long-lived Cape Verde hurricane that reached Category 5 strength (SSHS) three times and caused considerable damage and loss of life as it passed through the Caribbean Sea. Ivan developed from a large tropical wave accompanied by a surface low-pressure system that moved off the west coast of Africa on 31 August 2004. The development of the system continued and became tropical storm Ivan at 0600 UTC 3 September and a hurricane at 0600 UTC 5 September. After passing Grenada and moving into the southeastern Caribbean Sea, the hurricane's intensity leveled off until 1800 UTC on 8 September when a brief period of rapid intensification ensued. Reconnaissance aircraft data indicated Ivan reached its second peak intensity -- 140 kt and category 5 strength (SSHS) -- just 12 hours later. This was the first of three occasions that Ivan reached the category 5 level.

We choose the forecast period from 0000 UTC 8 Sept. to 0000 UTC 11 Sept. 2004 to examine effects of the central sea surface air pressure on predicting the hurricane track. For the control run (referred as CTL), the model started at 0000 UTC 8 Sep 2004 with the NOAA NCEP Global Forecast System (GFS) analysis fields as the model initial condition. For the central sea level air pressure experiment run (referred as SLP), only the observed central pressure was added to the initialization, using the GFS analysis as the first guess. The lateral boundary conditions for both simulations came from the GFS 6-hour forecasts. The same model physics options were used for the two experiments.

As shown in Figure 3, from run CTL, the hurricane central pressure at the initial time of 0000 UTC 8 Sept 2004 is about 998.7 hPa (obtained from the NOAA/NCEP GFS global large-scale analysis), which is ~15 hPa lower than normal conditions. Although this simulated pressure drop is much smaller than the real hurricane center air pressure depression (see below) and relatively weak for a hurricane, it still could be well captured with our proposed O_2-band radar systems. At 0000 UTC 8 Sept 2004, based on the report of the National Hurricane Center, hurricane Ivan was located at 12.0° N and 62.6° W, and the value of central sea level pressure of the hurricane is actually 950 hPa. This observation-based central pressure estimate was assimilated into the model analysis system. The assimilated initialization field shown in Figure 4 is used as the initial condition in run SLP. The value of the central pressure of the hurricane now is about 951.5 hPa, much closer to the observed
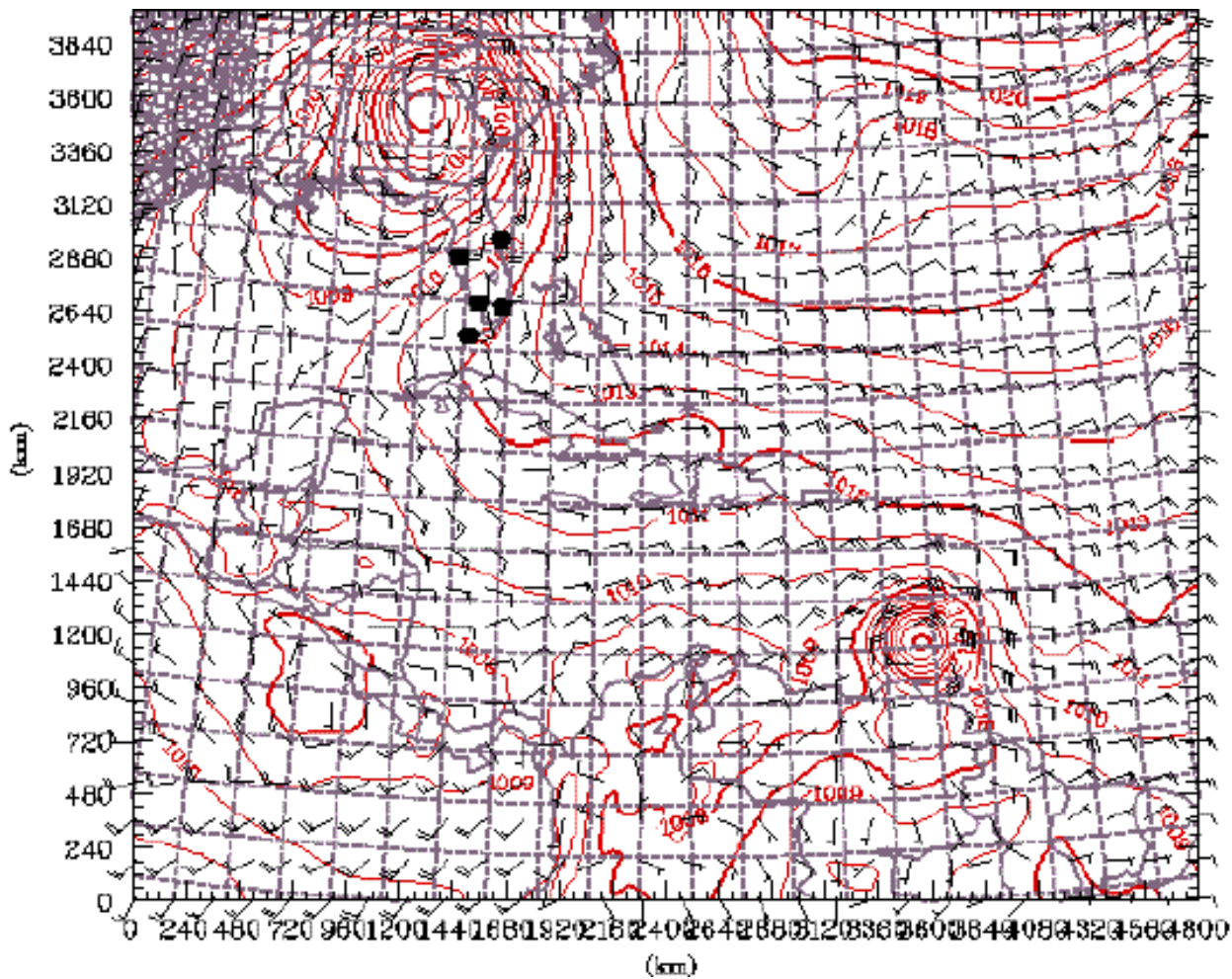
Fig. 3. The sea level air pressure at the initial time of 0000 UTC 8 Sep 2004 for the control run CTL. It is directly interpolated from GFS analysis.

950 hPa and within the error bar of observations. Compared to Figure 3, the change in the initial hurricane center sea level pressure is about 47mb, which significantly improves the predicted hurricane intensity.

The model was integrated for 72 hours at a time step of 15-seconds and used to estimate the storm track. It is not surprising that both of the experiments capture the hurricane track much better than the operational GFS global forecasting (Figure 5). This is mainly because the regional numerical model is non-hydrostatic with explicit cloud/ice-physics parameterizations, cloud-radiation interaction, as well as advanced turbulence schemes, and land-surface interaction. This kind of advanced regional model can better resolve multi-scale atmospheric processes, especially for organized convective cloud systems. A significant improvement in the predicted hurricane track resulted from the use of the observations of the central surface pressure in the initialization of SLP, as shown in Figure 5. The SLP experiment generated a more realistic hurricane track, especially for the first two forecasts. The results of our sensitivity tests suggest that it is possible to make better predictions of hurricane track by using surface pressure observations/measurements within the targeted tropical cyclone region.
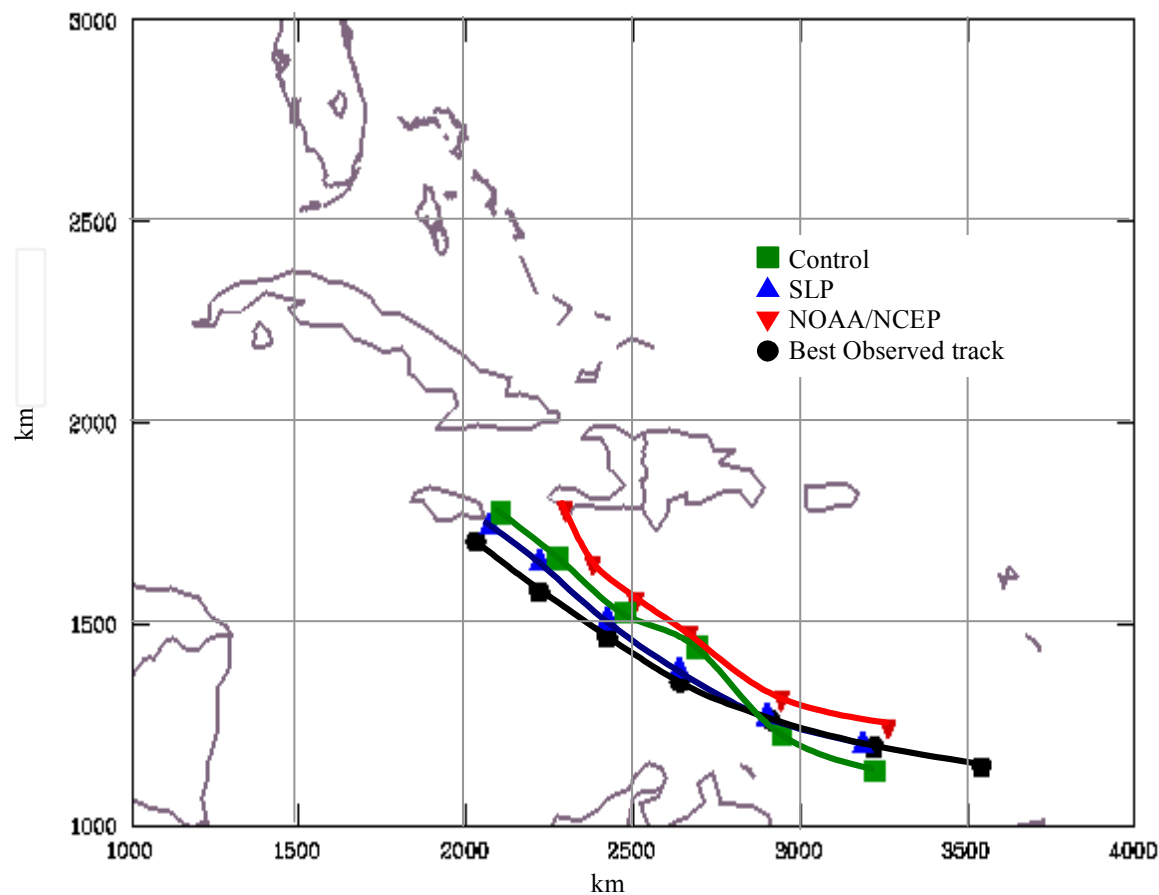
Fig. 4. The sea level pressure at the initial time of 0000 UTC 8 Sep 2004 for the experimental run SLP. The observed central pressure was used for the initialization with GFS analysis as the background.

2.3 Forecast improvements when pressure fields are ingested into model

The results of typical weather predictions for a tropical cyclone, using not only center sea surface air pressures but also large area pressure fields, is shown in Fig. 6 for 1996 hurricane Fran, which occurred from 0000UTC September 3 to 0060 UTC September 6, 1996 (Xiao et al. 2000). Due to the lack of data, the model standard run (control run; CTL curve) started with a location error of about 100km, and gradually deviated from the observed hurricane track (OBS curve) up to about 350km for the predicted landfall site. With pressure data and calculated wind fields as inputs, the assimilations with 54km (A80 curve) and 18km (B80 curve) spatial resolution significantly reduced the errors in predicted storm tracks. Comparing the 3 day forecasts, the high-resolution model (18 km, B80) had a small starting location error of about 10 km that increased to about 100 km at the predicted landfall site, and the low-resolution model (54 km, A80) had a starting error of about 35 km and predicted landfall with a 170 km error. Such greatly improved predictions could make hurricane preparation and evacuation much easier, especially for the high resolution forecast (B80) case.

Fig. 5. The predicted hurricane tracks from 0000 UTC 8 Sep 2004 to 0000 UTC 11 Sep 2004.
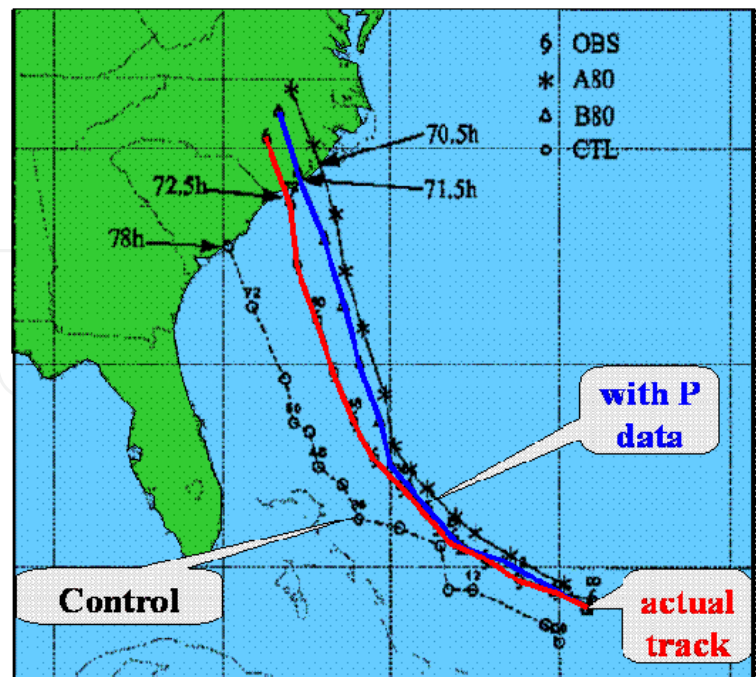
Fig. 6. Predicted tracks of 1996 hurricane Fran by CTL, B80, and A80, along with observations, from 0000 UTC 3 Sep to 0600 UTC 6 Sep. Predicted landing times are also indicated in the figure.

Storm intensity predictions can also be improved with knowledge about the storm center pressure, pressure gradients, and derived wind fields. As expected, the intensity of the B80 prediction is very close to observations at the landfall site (Xiao et al., 2000). The hurricane eye, rain band, and precipitation intensity determined from radar reflectivity simulations (a) and radar observations (b) are very similar (Figure 7). The similarity between these predicted hurricane intensity fields, using pressure fields as one of critical initial conditions, and fields based on observations is remarkable. Unfortunately, there have been no operational, or even experimental, surface air pressure measurements over open oceans
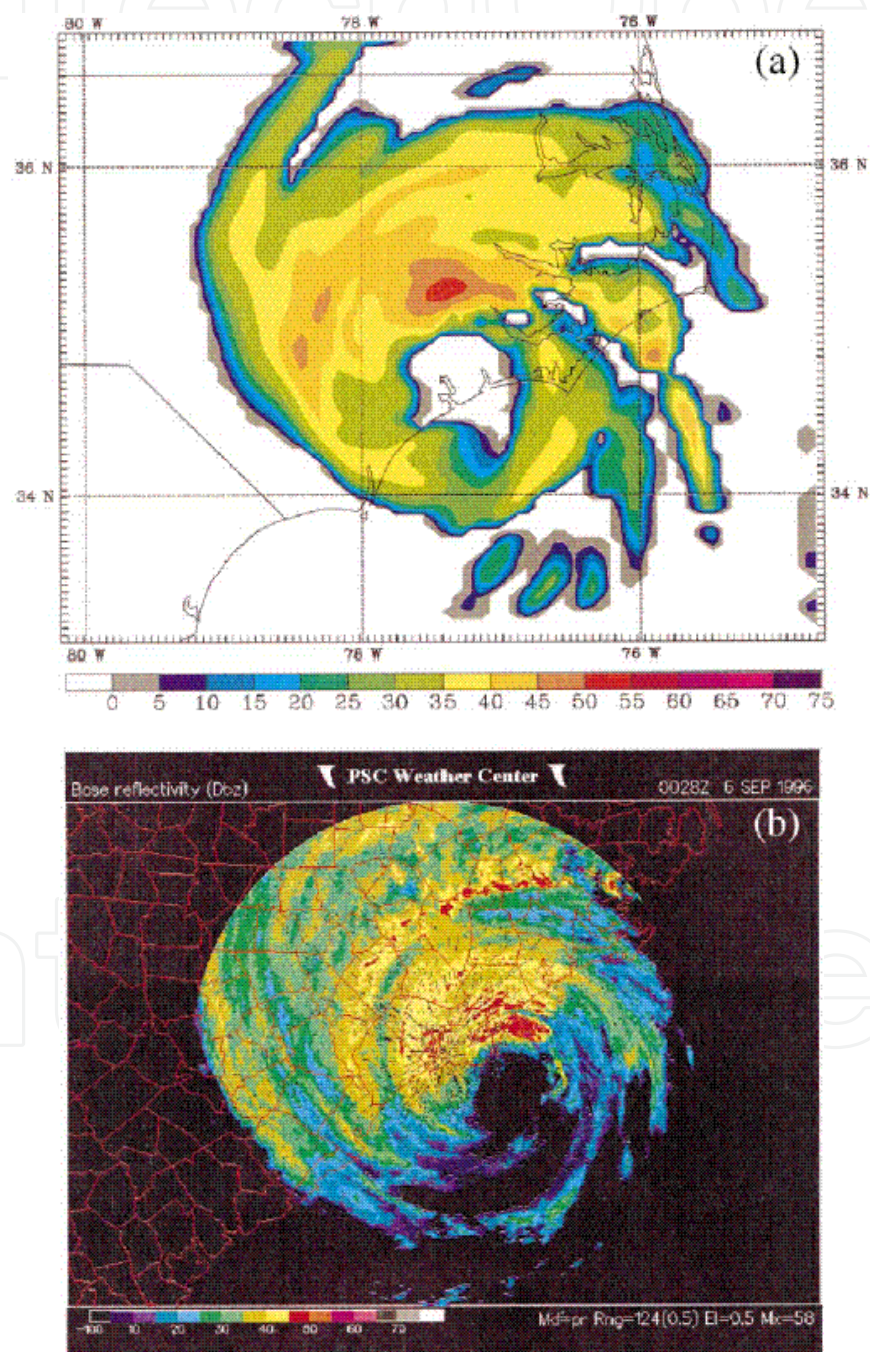
Fig. 7. Radar reflectivity (dBZ) (a) predicted by B80 at 0000 UTC 6 Sep 1996 and (b) captured at Wilmington, NC, at 0028 UTC 6 Sep 1996.

from both in-situ and remote sensing instruments, and thus it remains difficult to predict the tracks and intensities of tropical storms with high accuracies (within 100km landfall site for 3-day forecasts).

The results of the above simulations suggest that tropical storm forecasts of landfall and intensity at landfall may be improved by adding pressure field data consistent with the DiBAR measurement concept. With the pressure measurements of the center and whole field of tropical storms, our simulations using regional weather forecast models show that the prediction of hurricane tracks and intensities can be significantly improved. For the hurricane Fran case, model prediction reduces the landfall site errors from ~350km in the standard prediction to ~100km for 3 day forecasts, which could improve hurricane preparation and evacuation.

An operational airborne instrument could provide unprecedented barometric sampling in terms of spatial coverage and repeat rates. Assuming similar operational flights a DiBAR instrument would be expected to provide data at the same pressure resolution but much higher spatial density. If UAV is used, the cost of providing the needed barometric measurements could be significantly lower than that of current operations using in-situ techniques with the accompanying increase in personnel safety. Future space borne systems may further improve the pressure field sampling, albeit with a more coarse spatial resolution. Furthermore, the availability of these data could result in improved weather forecasts for catastrophic events and could significantly reduce human loss and property damage.

3. Measurement approach

The DiBAR instrument is based on the retrieval of the differential absorption near the O_2 line complex (frequencies: 50–56 GHz). This selection of frequencies provides large changes in absorption for the reflected radar signals as a function of the frequency of the radar due in part to the different atmospheric O_2 attenuation coefficients. In the atmosphere, O_2 is generally uniformly mixed with other gases. The O_2 in the column observed by the radar is proportion to column air mass, the column air mass is proportional to the surface air pressure, and the reflected power measured by the radar can be approximated as (*Lin and Hu* 2005)

$$P_r(f) = \left(\frac{P_T G_t G_r \lambda^2}{(4\pi)^3} \right) \left(\frac{\sigma^0(f)}{r^2} \right) \exp\left(-\frac{2\alpha_o M_o P_o}{g} - 2\alpha_L L - 2\alpha_v V \right) \tag{1}$$

where the first term in equation (1) includes frequency dependent characteristics of the radar, which must be determined by instrument calibration: P_T is the transmitter power and G represents the transmitter and receiver antenna gain. The second term includes changes in the surface reflectivity, σ^0, over the radar frequency, and the last term represents the atmospheric absorption, where M_0 is the mixing ratio of O_2 to total air and P_o is the surface pressure. Thus, if the frequency response of the radar is well characterized from 50 -56 GHz, and the absorption characteristics due to liquid water and water vapor, and spatial resolution of the radar are similar over this range of frequencies, then the ratio of the radar received powers from two frequencies is then,

$$\frac{P_r(f_1)}{P_r(f_2)} = \left(\frac{C(f_1)}{C(f_2)}\right) \exp\left(-\frac{2(\alpha_o(f_1) - \alpha_o(f_2))M_o P_o}{g}\right) \tag{2}$$

where C(f) is the frequency dependent radar characteristics. Further, if we define the differential absorption index, $Ri(f_1, f_2)$, as the logarithm of the radar return ratio shown in equation (2), then the surface pressure can be written as,

$$P_o = \left(\frac{2(\alpha_o(f_1) - \alpha_o(f_2))M_o}{g}\right)^{-1} \ln\left(\left(\frac{C(f_2)}{C(f_1)}\right)\left(\frac{P_r(f_1)}{P_r(f_2)}\right)\right)$$

$$P_o = \left(\frac{2(\alpha_o(f_1) - \alpha_o(f_2))M_o}{g}\right)^{-1} \left(Ci(f_1, f_2) + Ri(f_1, f_2)\right) \tag{3}$$

or defining terms for a linear relationship between Ri and P_o,

$$P_o = C_0(f_1, f_2) + C_1(f_1, f_2)Ri(f_1, f_2) \tag{4}$$

The term $C_0(f_1, f_2)$ includes the instrument residual calibration error. The differential absorption index, $Ri(f_1, f_2)$, is the logarithm of the ratio of the radar return exclusive of the frequency response of the radar. From equation 4, it can be seen that a simple near-linear relationship between surface air pressure and the differential absorption index is expected from the O_2 band radar data. The linear relationship between Ri and the surface pressure was firstly suggested by the results of modeled differential absorption for several frequencies in the range of interest here (*Lin and Hu* 2005). Further, *Lin and Hu* 2005 suggest that the accuracy of instantaneous surface air pressure estimations from the measured Ri could reach 4 – 7 mb. However, the O_2 absorption increases at higher frequencies and the receiver Signal to Noise Ratio (SNR) may limit the retrieval accuracy as this loss increases. For a fixed transmit power the optimum frequencies for the surface pressure measurement will depend on the received power, which depends on the atmospheric loss and surface reflectivity. The flight testing of the DiBAR instrument discussed in Section 4 is intended to measure the atmospheric attenuation as a function of frequency and the differential absorption index $Ri(f_1, f_2)$. These measurements can then be compared to predicted values to assess the measurement approach and the affect of receiver noise on the measurement of barometric pressure.

In addition to the above analysis a multiple layered atmospheric microwave radiative transfer model was also employed to simulate the atmospheric loss. The technique used to simulate the propagation of radar signals within the atmosphere is based on a plane-parallel, multiple layered atmospheric microwave radiative transfer (MWRT) model that has been used to determine cloud liquid/ice water path, column water vapor, precipitation, land surface emissivity and other parameters over land and oceans (Ho et al., 2003; Huang et al., 2005; Lin & Rossow, 1994, 1996, 1997; Lin et al. 1998a, 1998b; Lin & Minnis, 2000). To avoid complexities of microwave scattering by precipitating hydrometeors and surface backscattering, this study deals only with non-rain weather conditions and homogeneous backgrounds (such as sea surface). Thus, transmission and absorption of radar signals within each atmospheric layer are the major radiative transfer processes considered in the model calculations. For the absorption process, this MWRT model carefully accounts for the

temperature and pressure dependences of cloud water and atmospheric gas absorptions (Lin et al., 2001). At microwave wavelengths, temperature dependences of gas and water absorptions are significant, and produce some difficulties for MWRT modeling. The several models available to account for gas absorption differ mainly in their treatment of water vapor continuum absorption. The Liebe model i.e., MPM89 was used here (Liebe, 1989). It yields results that differ negligibly from those of the (Rosenkranz, 1998) model at the O_2 bands. Liquid water absorption coefficients were calculated from the empirical water refractive index formulae of (Ray, 1972), which agree well (relative differences < 5%) with those from (Liebe et al., 1991) for T > –15° C. For colder clouds, the uncertainties in the absorption coefficients could be larger by more than 15% (Lin et al., 2001) because of a lack of direct measurements of the refractive index.

Current MWRT model is consistent of 200 constant-thickness layers from surface to 40km. There is virtually no gas absorption above the modeled top-of-atmosphere (TOA) at our considered spectra. The atmospheric profiles of temperature, pressure, humidity and gas amount are obtained from NOAA 1988 (NOAA'88) global radiosonde measurements. This NOAA'88 data set is widely used in radiation simulations and satellite remote sensing (e.g., Seemann et al., 2003) and covers both land and oceans. The data set has more than 5000 profiles, and about 1/3 of them are for cloudy skies. In cloudy cases, the NOAA'88 profiles can have up to two layers of clouds. Thus, the simulated results represent both clear and cloudy conditions. Since the model TOA (40km) height is much higher than that of radiosonde measurements, whenever there are no radiosonde upper atmospheric observations, interpolated climatological values of the upper atmosphere (McClatchey et al., 1972) are used. The weighting functions for the interpolation are decided from the surface air temperatures and pressures to meet the radiosonde measured weather conditions. In order to have large variations in surface air pressure, for each NOAA'88 measured profile, the surface pressure is randomly shifted by a Gaussian number with standard deviation 12mb, and the ratio of the shifted surface air pressure to the measured surface pressure is calculated. The atmospheric pressures in the measured profile above the surface are, then, adjusted to the values using the same ratio as that of the surface pressure.

For the analysis in this section, the radar system is assumed to fly on an aircraft at 15 km altitude with velocity 200 m/s, downward-looking and having a beamwidth of 3°, which produces a footprint of 785 m. The NOAA hurricane reconnaissance aircraft generally fly above 10 km height through and/or over hurricanes. Since this study is the first step in the model simulations for the radar system to show feasibility of the radar remote sensing for sea surface barometry, the 15 km altitude simulations provide us sufficient theoretical and technical insights for the radar sea surface pressure measurements. For other altitudes, the radar retrievals should have similar accuracy to those simulated here. During our simulation, since all wavelengths used in the radar system are very close to each other, we assume the surface reflection (or σ^0) to be the same (11 dB) for all frequency channels (Callahan et al., 1994). As we have showed in the previous section, the absolute magnitude of the surface reflectivity is not very important for surface pressure estimation as long as the spectrum dependence of σ^0 within the O_2 bands is negligible.

Simulated signals are analyzed in the form of relative received power (RRP), i.e., the ratio of the received and transmitted powers of the considered radar system. Since the system works at the O_2 absorption bands, the relative received powers are generally weak. Certain signal

coding techniques for carrier frequencies, correlators for signal receiving and long-time (0.2s) averages of received powers are useful components for consideration for the radar system. Preliminary studies have disclosed advantages from a number of commonly employed radar techniques.

The radar-received signals reflected from sea surfaces, i.e. RRP values, used in this section are simulated through the complicated MWRT calculations discussed previously. With the RRP values, we calculate the radar differential absorption index, Ri, defined in equation 4. As shown above, the index and sea surface air pressure have a near-linear relationship, which points out the basic directions and sensitivities for surface air pressure remote sensing.

Atmospheric extinctions (or attenuations) vary dramatically at the O_2 band radar frequencies between 50.3 and 55.5 GHz. At the lowest frequency (50.3GHz), the atmospheric extinction optical depth is about 0.5, and at the highest frequency (55.5GHz), the optical depth goes sharply up to about 9. These two frequency cases represent the two extreme ends of weak and strong, respectively, atmospheric O_2 absorptions for our considered active microwave remote sensing of sea surface barometric pressure. With a weak O_2 absorption (i.e., small optical depth) radar signals would have significant influence from environments, such as atmospheric water vapor, cloud water amount and atmospheric temperature profile but transmitted powers used might be lower. While the atmospheric O_2 absorption is too strong, most of radar-transmitted powers would be close to attenuation, and small changes in surface air pressure (or column O_2 amount) would not produce significant differences in the received powers. This might be offset somewhat by using higher transmitted power. Thus at constant transmitter power levels, wavelengths with moderate to reasonably strong O_2 absorptions in the atmosphere are expected to serve our purpose best by giving a reasonable compromise between transmission and visibility.

Figure 8 shows examples of atmospheric extinction optical depths counted from TOA under clear conditions using the standard profiles (*McClatchey et al.* 1972). The three different color
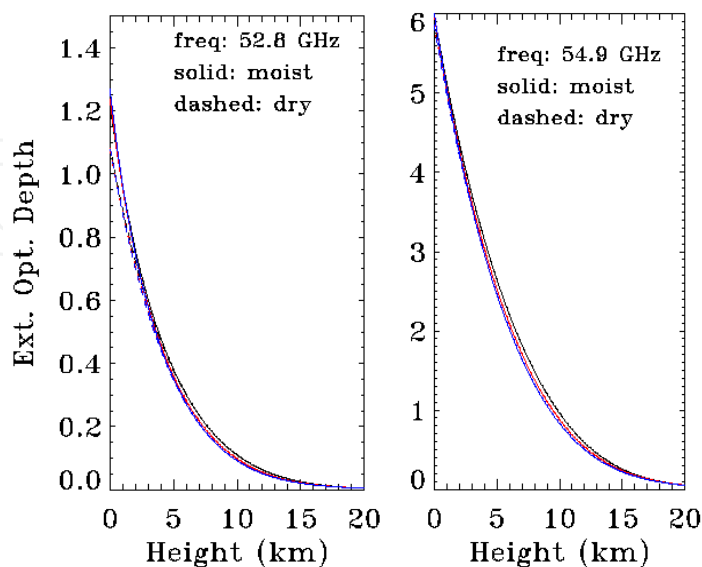

Fig. 8. Atmospheric extinction optical depths for various atmospheric temperatures and moisture levels at 52.8 and 54.9 GHz.

curves represent atmospheric surface temperatures of 280, 290 and 300K, respectively. It can be seen that these curves are very close each other, indicating atmospheric temperature effects are minimal. For channel 2 (i.e. 52.8GHz, left panel) cases, the optical depths for moist atmospheres (solid curves) with 40mm column water vapor are about 1.25 and only 0.1 higher than those of dry atmospheres. At 54.9GHz (right panel), the optical depths are increased considerably to about 6, and different temperature and moisture conditions have little effect on the total extinctions. For this frequency, the atmospheric extinctions of radar received signals due to double atmospheric path lengths reach about 50dB. This may require enhancements to the radar signals to control end to end noise, as mentioned before.

For tropical meteorological cases, such as hurricane cases, the changes in temperature and moisture profiles are even much smaller than those shown in the figure due to limited temperature and humidity conditions for the tropical storm development. To test accuracies of surface pressure measurements, a 15 dB SNR (signal-to-noise ratio) for radar-received signals is assumed for this primary study.

Figure 9 shows the simulated relationship between the differential absorption index (the logarithm of the radar return ratio of relative received powers at wavelengths 53.6 and 54.4 GHz and sea surface air pressure. Each point in the figure represents one adjusted NOAA'88 profile. As discussed above, good linear correlations of the two variables are further established by these simulations. A linear regression gives the root mean square (rms) error in sea surface air pressure estimates about 7.5 mb, which may be suitable for many meteorological uses. For frequencies of 53.6 and 54.9 GHz (Figure 10), simulated results (5.4 mb) are close to current theoretical O_2 A-band results. The best results (in Figure 11) we found are those from the differential absorption index 52.8 and 54.9GHz. The rms error in this case is about 4.1 mb. The tight linear relation between the sea surface air pressure and differential absorption index provides a great potential of remote sensing surface air pressure from airborne radar systems. Note that in Figs. 9-11, the dynamic range of sea surface barometric pressure is only from ~ 960mb to ~1050mb. The low end of the dynamic
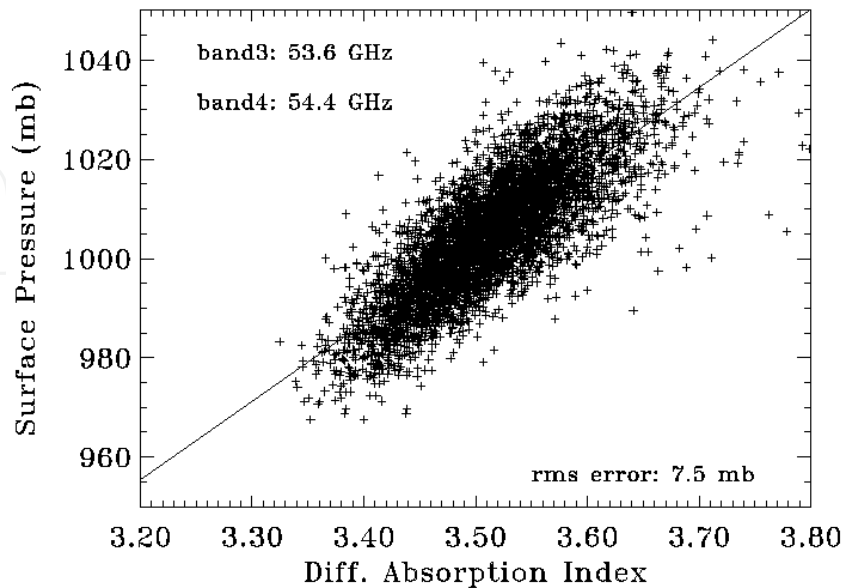

Fig. 9. Simulated relationship between the differential absorption index, the logarithm of the radar spectrum ratio at wavelengths 53.6 and 54.4 GHz , and surface air pressure.
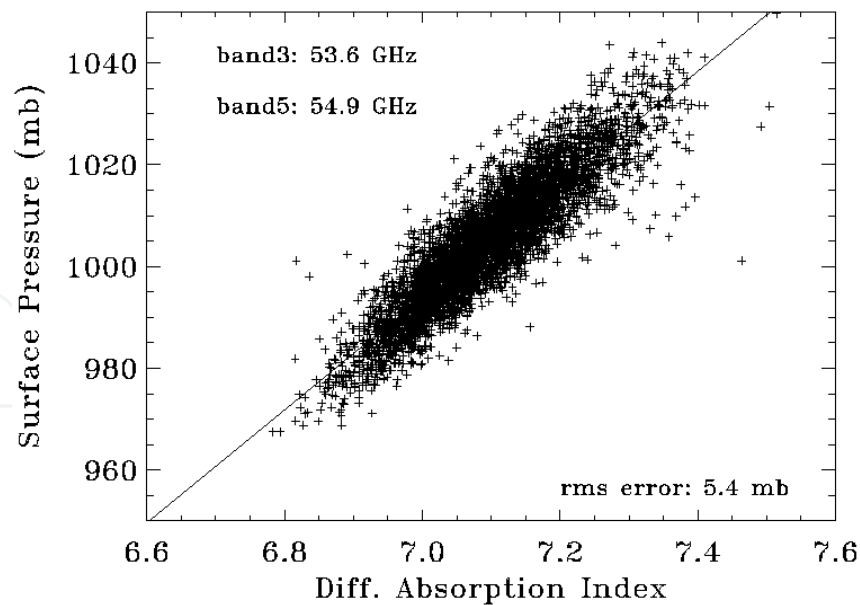
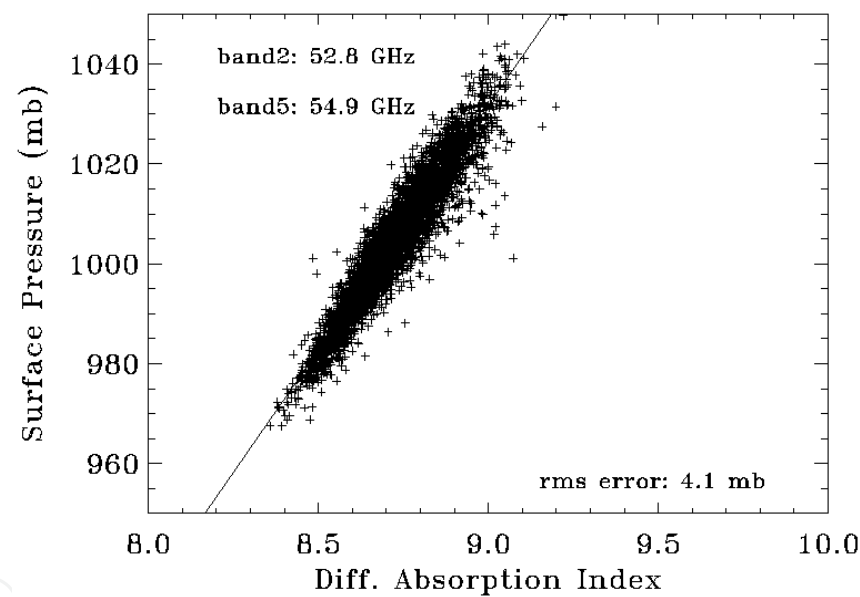Fig. 10. Similar to Fig. 9, except frequencies are changed to 53.6 and 54.9 GHz.

Fig. 11. Same as Fig. 10, except for 52.8 and 54.9GHz.

range of the sea surface pressure is significantly higher than some sea surface air pressures of hurricane centers. NOAA 1988 profiles were measured in generally average weather and meteorological environments, and were not taken from tropical storm cases. Thus, there were no extreme low sea surface air pressures in the NOAA data set. Actually, for tropical storm cases, the signal strength and SNR of the radar measurements at all O_2 band channels would be higher than those in normal conditions due to low atmospheric radar attenuation caused by low O_2 amounts (or the low hurricane center pressures). Also, the hurricane centers are generally clear skies. So, the accuracy of radar retrievals of the sea surface barometric pressure for hurricane center cases would be higher than those shown in the figures. The key to reach high accuracies of sea surface barometric pressure measurements is to have a high SNR of radar received powers reflected from sea surfaces.

This theoretical and modeling study establishes a remote sensing method for sea surface air pressure. Simulated results show that with an airborne radar working at about 53~55GHz O_2 absorption bands, the rms errors of the radar surface pressure estimations can be as small as 4~7mb. The considered radar systems should at least have 2 frequency channels to obtain the relative received power ratios of the two wavelengths. For the best simulated combination of 52.8 and 54.9 GHz channels, the power loss of radar received signals due to dual atmospheric path length absorptions could be as high as about 50 dB. High signal-to-noise ratios for radar reflected powers after these atmospheric absorptions will require modern radar technologies. In addition, careful radar design to insure stable instrument gain will be required.

4. DiBAR demonstration instrument

The goal in developing the demonstration instrument was to use commercial-of-the-shelf hardware wherever possible to develop the capability to collect differential absorption data that would verify the simulated differential absorption results, and to allow various measurement approaches to be assessed. An important operational characteristic for the radar, and determining factor in most design tradeoffs for the DiBAR system, is the SNR. The optimum channel to use in the O_2 absorption band from 50 ~ 56 GHz is a function of the radar SNR, which depended on the surface reflectivity and the total atmospheric absorption. Thus, rather than selecting a set of frequencies bases on the microwave atmospheric absorption model, the demonstration instrument will have the flexibility to vary the measurement frequencies, and even to measure the differential absorption from 50 to 56 GHz and allow multiple processing and data analysis strategies to be evaluated for the same data set.

The basic instrument concept utilizes a Vector Network Analyzer (VNA) and a millimeter wave Up/Down Converter subsystem to enable operation from 50 ~ 56 GHz. The millimeter wave Up/Down Converter will translate the VNA measurements to the O_2 absorption band, and provide very flexible signal processing options. As shown in Figure 12, the Up/Down Converter provides a millimeter power amplifier for the transmitter and a Low Noise Amplifier (LNA) for the receiver. The transmit power is selectable but the maximum is limited by the Q-band output amplifier to +14 dBm. The maximum transmit power and the receiver noise figure, 5.3 dB, will establish the SNR for our selected flight altitude. Our analysis indicates that for altitudes below 1000 m the SNR will be sufficient to verify the differential absorption across the O_2 absorption band. The transmit power can also be reduced during the flight to assess the impact of SNR on various data analysis approaches. Finally, to maximize isolation and eliminate the need for a Q-band transmit/receive (T/R) switch, the demonstration instrument transmitter and receiver are each fitted with an antenna.

The DiBAR demonstration instrument is extremely versatile and can be operated in several modes to emulate a wide range of radar modes and processing concepts. Several modes of operation can be used to collect absorption band data to increase probability of success and provide additional insight into the concept of differential absorption. The anticipated data sets will also provide insight into other phenomenon, at these frequencies, such as sea surface scattering. The instrument can be retrofitted with microwave switches to allow hardware gating, if required, to reduce any radar return other than the ocean surface. This option is not presently implemented.
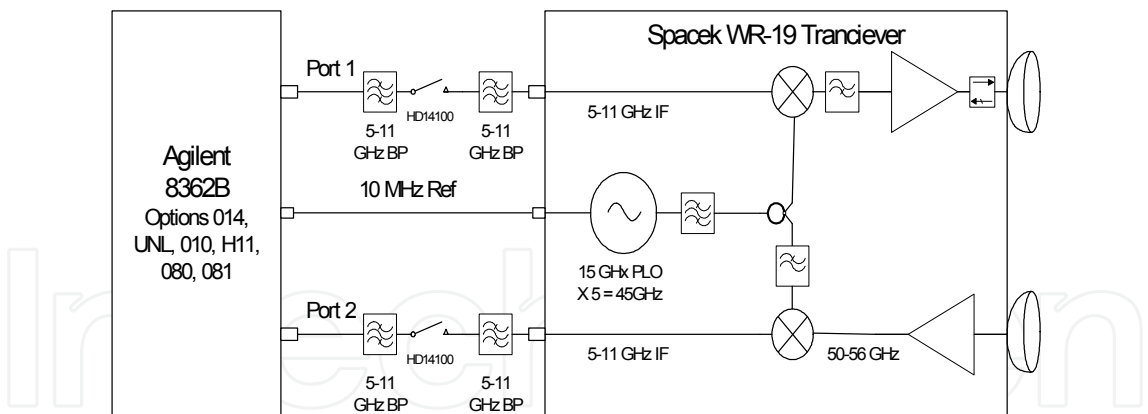
Fig. 12. DIBAR demonstration instrument block diagram.

For the data discussed here, the DiBAR instrument was operated in a stepped Continuous Wave (CW) mode using Fourier transform and windowing to produce software gating in the time domain. This processing minimized the effect of radar returns other than from the sea surface, or leakage between the transmitter and receiver.

4.1 Preliminary functional testing

Laboratory functional testing of the system such as, characterization of system linearity, noise figure, antenna gain, and isolation between antennas has been completed and reported elsewhere (Lawrence et al. 2007; Lin et al., 2006). Results of these tests were nominal with two minor exceptions. The frequency response of the Up/Down Converter, shown in figure 12, varied over the frequency range of 50 and 56 GHz by more that 12 dB. This change with frequency was larger that expected. However, it has been assumed that low altitude DiBAR data would be used to characterize the frequency response of the instrument during the flight tests. Therefore, as long as frequency response is stable, this should not affect the DiBAR demonstration flight tests. The leakage from the transmitter to the receiver within the Up/Down Converter enclosure was larger than mutual coupling between antennas. The impact of this leakage is minor. Our stepped CW measurement approach allowed software gating to suppress this term as long as the range to the target is more than about 10 to 15 m. Again, this had no impact on flight tests.

The assembled DiBAR demonstration radar is shown in figure 13 during a quick test using a water tower as a target to verify the operation of the radar. The DiBAR instrument collected 16001 stepped CW measurements for frequencies from 53 to 56 GHz. The Fourier transform of these data then results in a time domain representation of the radar return as a function of range. The resulting time domain data is shown in figure 14 and the large return from the water tower as well as the internal leakage term can clearly be seen in the figure.

The data in figure 14 may be helpful in illustrating the DiBAR measurement approach. The DiBAR instrument must provide precision measurements of the variation in the radar return as a function of frequency. Using a similar stepped CW measurement approach over the ocean, we can transform the data to the time domain, and then use windowing to minimize the effects of clutter. The windowed time domain data can then be transformed back to the frequency domain to measure the differential absorption index. An important assumption for our test flight planning is that the frequency response of the instrument will be
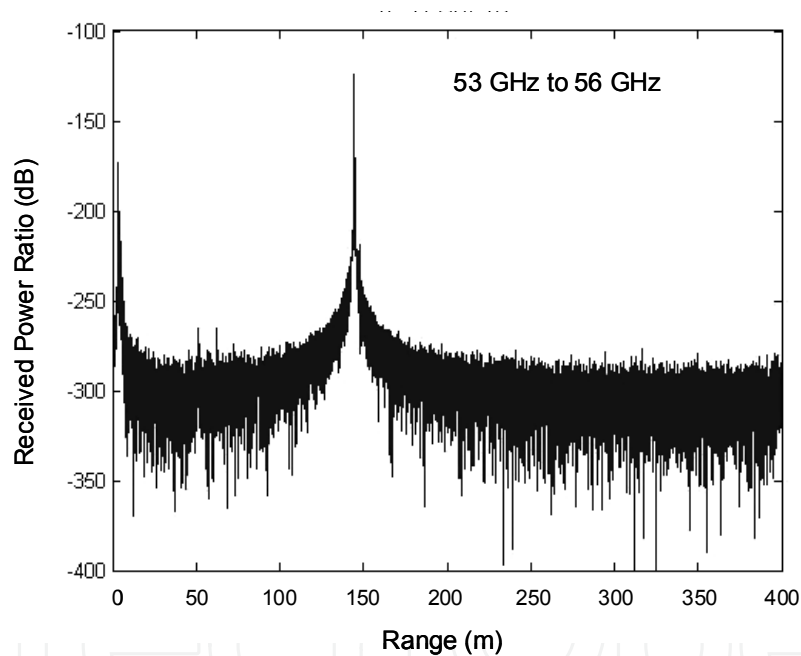
Fig. 13. DiBAR Demonstration Radar

Fig. 14. Radar return from water tower vs. range

characterized by comparing stepped CW data at various flight altitudes. This of course assumes stability of the instrument frequency response. In order to verify the stability of the frequency response, the DiBAR instrument was moved into an anechoic chamber to

measure the backscatter from a conductive sphere in a stable and controlled environment. Unfortunately, the available chamber was not designed for millimeter wave frequencies, so precision radar cross section measurements or absolute calibration of the DiBAR instrument was not possible. However, while clutter was apparent in the radar measurements, the facility did provide a stable environment and was useful for the primary objective of characterizing the stability of the instrument.

The data was collected in the stepped CW mode using 16001 points from 50 to 56 GHz over several hours. The time domain result of a measurement of a 35.5 cm diameter sphere is shown in figure 15. The sphere can be seen at a range of approximately 22 m. The leakage term appears near zero range and the back wall of the facility is only a few meters further downrange than the sphere. Windowing was used to reduce the error due to these contaminating signals and the data is then transformed back to the frequency domain. Assuming the sphere is stationary, any change in the measured response can be attributed to variation in the end-to-end frequency response of the DiBAR demonstration instrument.
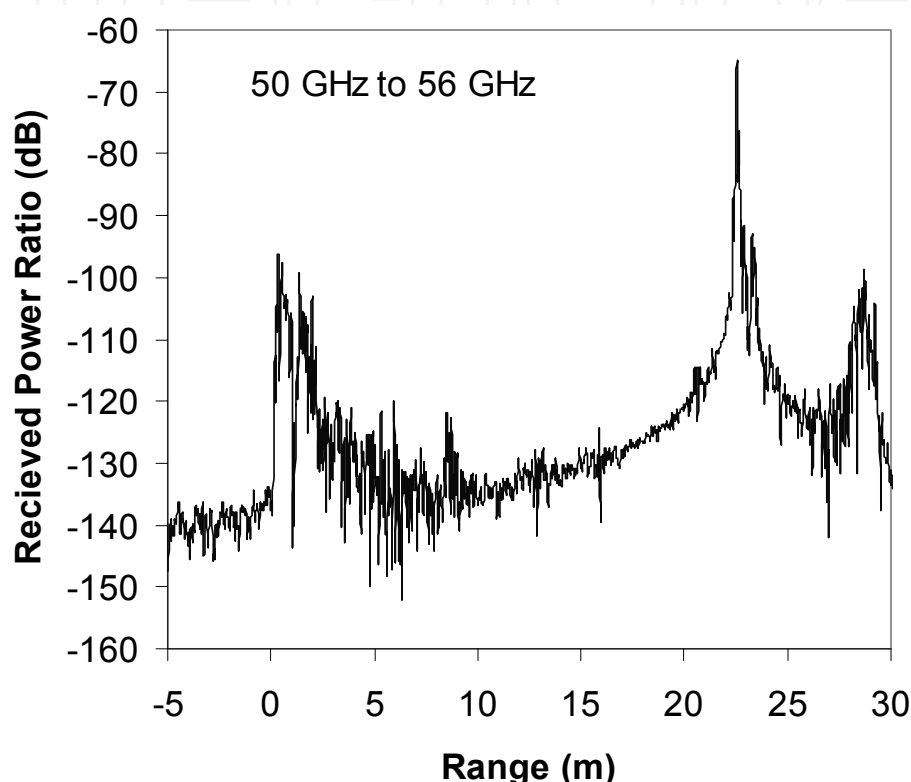
Fig. 15. Radar return from sphere vs. range

4.2 DIBAR flight test results

The initial flight-testing to verify the differential loss was accomplished utilizing a helicopter that provided several test flights over water in varying atmospheric and sea conditions. Several modifications to the DiBAR instrument were required for these tests. The integration of the DiBAR instrument on board the helicopter required the high gain antennas to be replaced with smaller horn antennas. The reduction in antenna gain results in reduced system dynamic range, and limits the maximum altitude where sufficient signal to noise ratio is available for useful pressure measurements. To minimize the impact of the antenna modification, the frequency sweep was increased from 53-56 GHz to 50-60 GHz for these flights. While the spectral response of the DiBAR instrument decreases above 56 GHz, the increased O_2 attenuation at these frequencies may be useful for the lower altitude operations. Analysis using an instrument model developed from laboratory testing and the microwave absorption model described in (Lin & Hu, 2005, Lawrence et al., 2007) suggests that this configuration of the instrument will provide an estimate of the differential O_2

absorption for an altitude of approximately 3000 feet (ft). Note that within US aviation industry aircraft altitude is reported in feet. Since this is the value recorded by the flight crew, altitude will be reported in feet in this description.

The demonstration DiBAR instrument was installed on a helicopter (Figure 16) for several test flights. Data was collected with in-situ estimated barometric pressure ranging from 1007 to 1028 mb. At each measurement site, the DiBAR instrument made three to five measurements of radar return for frequencies from 50 to 60 GHz. These measurements were performed while the helicopter was in a hover and each measurement set included altitudes from 500 to 5000 ft. These measurements were performed at each altitude with the helicopter at nominally the same location. The 500 ft altitude measurements for each measurement set was used to provide correction for sea surface reflectivity variations and spectral calibration of the instrument.

Fig. 16. DiBAR Instrument Installed in vehicle for initial flight tests.

The results for a data set performed on a day with an in-situ estimated barometric pressure at the measurement location of approximately 1018mb are shown in figure 17. DiBAR data for 2000, 3000, and 5000 ft altitudes is shown, as well as the modeled radar return. Three DiBAR measurements were performed at each altitude, and are indicated by the three different symbols in Figure 17. The predicted radar return (solid curve) is estimated using the radar equation for an extended target (sea surface) and the microwave absorption model adapted from (Lawrence et al., 2007; Lin & Hu, 2005). The measured transfer function of the DiBAR instrument was then combined with these models to estimate the expected radar return, shown in Figure 17 as the solid curve. The DiBAR measurements for each altitude are very repeatable, suggesting that the DiBAR instrument and the sea surface scattering characteristics were sufficiently stable. The reduced radar return as the measurement frequency increases can clearly be seen in Figure 17. This reduction is partially due to the increased O_2 attenuation discussed in section 3.
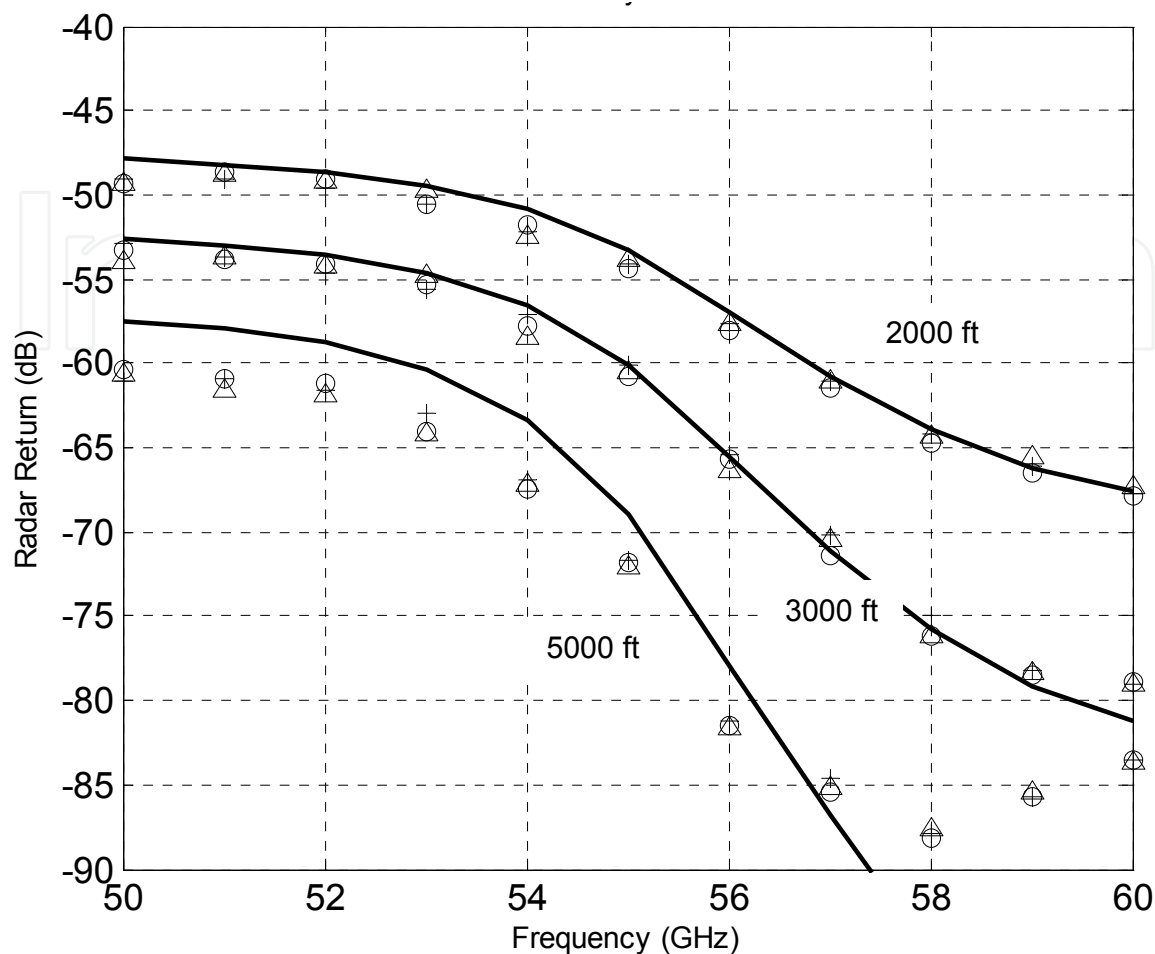
Fig. 17. Comparison of DiBAR measured return and model predictions

The measured results agree very well with the model for 2000 ft altitude measurements. The results for 3000 ft also agree well with the model for frequencies from 50 to 58 GHz. The difference between the measured and predicted values above 58 GHz is likely due to the noise floor of the modified DiBAR instrument. That is, due to the reduced antenna gain the signal to noise ratio of the DiBAR is insufficient at frequencies above 58 GHz at 3000 ft altitude and above 56 GHz at 5000 ft altitude. It appears that the optimum trade off between sufficient O_2 absorption (path length) and the noise floor of the DiBAR instrument for these flights occurs at an altitude of approximately 3000ft. Future flights with the high gain antennas will not have this limitation.

DiBAR data for 3000 ft from three difference days are shown in Figure 18. Three measurements are indicated for each day (symbols) as well as the predicted values (solid line). The increase in attenuation with increasing frequency can be seen in the data for all three days. Further, the attenuation appears to increase with increasing barometer pressure as would be expected. The difference between barometric pressures for each day is approximately 10 mb. While no statistical analysis was performed, the variation in the measured attenuation above 57 GHz appears to be on-the-order of the variation between each day. That is, the measurement-to-measurement variation was on the order of ± 5 mb
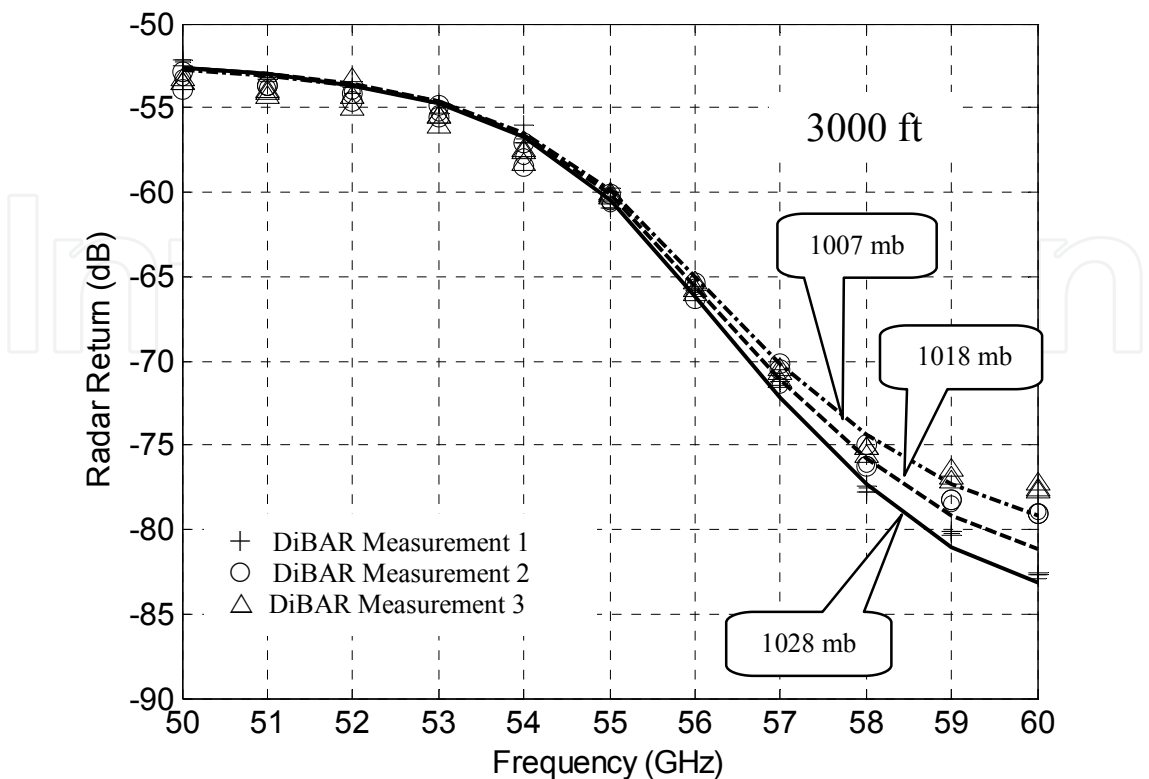
Fig. 18. Measured radar return and model predictions for three pressure days.

for the 3000 ft altitude data. The stability of these measurements over several minutes indicates that sea surface scattering can be assumed constant for these conditions. As discussed in Section 3 this increase in attenuation is expected to result in a linear change in differential absorption, Ri(f1,f2) defined in equation 4.

The differential absorption index is also provided by DiBAR measurements. The DiBAR demonstration instrument measures the radar return over the entire frequency band from 50 to 60 GHz. However, the differential attenuation index can be extracted from the data where the radar signals are sufficiently above the noise floor. For example, the differential absorption for f1= 53 GHz and f2=58 GHz, or Ri(53,58), can be found from Figure 18 by

subtracting the radar return for 58 GHz from that for 53 GHz. Figure 19 shows Ri(53,58) measured at altitudes of 1000, 2000, 3000, and 4000 ft. The measured data for the three pressure days are shown in the figure as well as the predicted Ri(53,58) using the instrument model and microwave atmospheric attenuation model discussed above. The figure illustrates the affect of increasing altitude. As the altitude increases the increased path length increases proportionality constant between Ri and P_o in equation (4). Thus, ignoring the receiver SNR, a less precise estimate of Ri is required for the same surface pressure precision at higher altitudes. Conversely, at 1000 ft larger changes in barometric pressure would be required to produce a detectable change in Ri. This demonstrates the impact of the reduction in antenna gain and limiting the useful measurement altitude to 3000 ft. However, the differential absorption index shown in Figure 19 agrees well with the predicted values for Ri, through 3000 ft altitude.
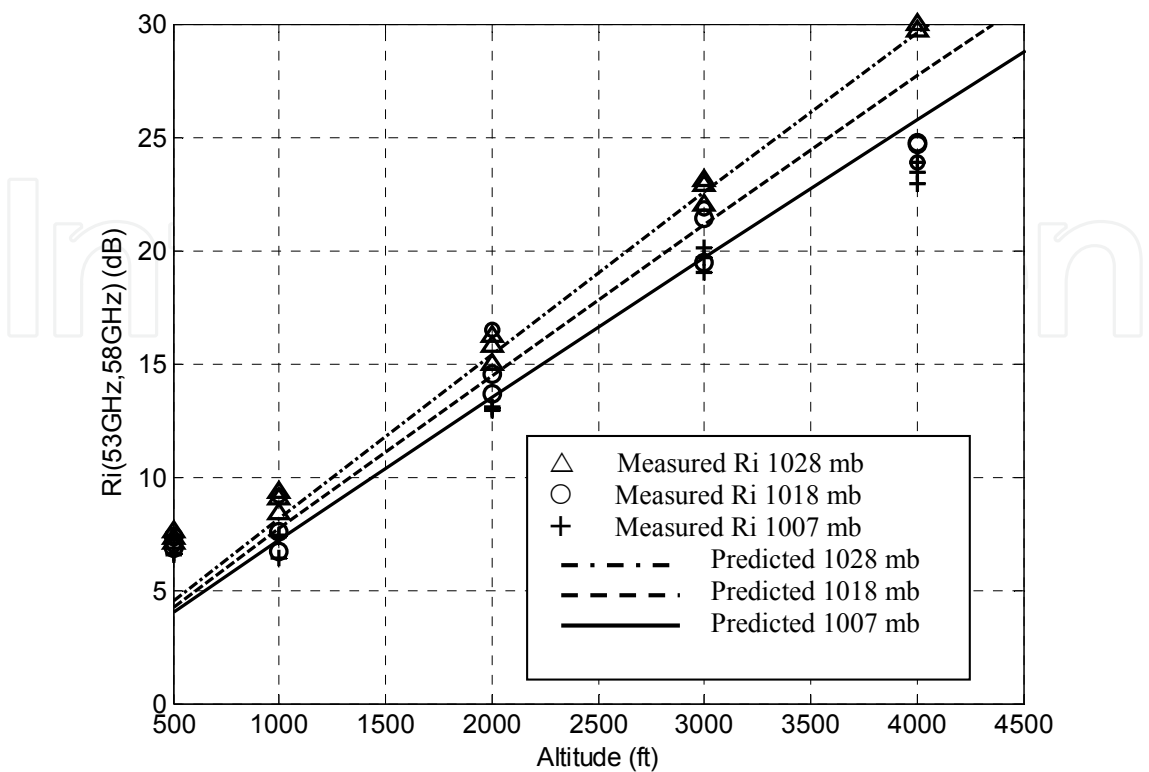
Fig. 19. DiBAR derived and predicted differential absorption coefficients.

5. Conclusions

The goal of the initial flight testing was to demonstrate differential radar measurement approach. The DiBAR measurements for the Chesapeake Bay at multiple altitudes demonstrated very good agreement between measured and predicted results for altitudes below approximately 3000 ft and for frequencies below 56 GHz. In addition, multiple measurements at these altitudes indicate little change over several minutes. This suggests that changes on the surface reflection coefficient over these time scales can be ignored for these surface conditions and spatial resolution. As expected, above 3000 ft the reduced antenna gain resulted in insufficient signal to noise ratio. However, the measured differential absorption index was in general agreement with the modeled values. Further, although beyond the scope of these initial flight tests, variations in the DiBAR measurements for 3000 ft measurements appear to be in the range ± 5 mb. These results are encouraging and consistent with our accuracy goal. Future flight testing should include an assessment of the barometric pressure measurement for high altitude and future satellite operations.

The initial flight testing described above successfully demonstrated the measurement approach. To fully demonstrate the measurement of surface level pressure will likely require flight data at altitudes between 5 kft and 15 kft using the original high gain antennas. An onboard calibration system should also be developed to eliminate the need for low altitude data to correct for changes to the spectral response of the instrument. In

addition, while the existing demonstration DiBAR instrument is suitable to demonstrate the concept, a radar processor should be developed specifically for the differential absorption measurement to eliminate the need for the PNA. This would substantially reduce the weight and size of the instrument. This modification should not only eliminate the PNA, but should also be designed to enhance the stability of the instrument and enable the pulse operation to eliminate one of the antennas. While eventually funding will be required to develop an operational DiBAR instrument capable of operation at altitudes of 40 kft, these improvements may lead to moderate altitude flight opportunities.

6. References

Barton, I.J., and Scott, J.C. (1986). Remote measurement of surface pressure using absorption in the Oxygen A-band, *Appl. Opt.*, 25, 3502-3507.

Callahan, P.S., Morris, C.S. and Hsiao, S.V. (1994). Comparison of TOPEX/POSEIDON σ_0 and significant wave height distributions to Geosat, *J. Geophys. Res.*, 99, 25015-25024,.

Chou M-D (1990). Parameterization for the absorption of solar radiation by O2 and CO2 with application to climate studies. *J. Climate*, 3, 209-217.

Chou, M-D. (1992). A solar radiation model for climate studies. *J. Atmos. Sci.*, 49, 762-772.

Chou M-D and Suarez, M. J. (1994). *An efficient thermal infrared radiation parameterization for use in general circulation models*, NASA Tech Memo 104606.

Flower, D.A., and Peckham, G.E. (1978). *A microwave pressure sounder*, JPL Publication 78-68, CalTech, Pasadena, CA.

Ho, S.-P., Lin, B., Minnis, P., and Fan T.-F.(2003). Estimation of cloud vertical structure and water amount over tropical oceans using VIRS and TMI data, *J. Geophys. Res.*, 108 (D14), 4419, doi:10.1029/2002JD003298.

Huang, J., Minnis, P. , Lin, B., Yi, Y., Khaiyer, M.M., Arduini, R.F., Fan, A., Mace, G.G. (2005). Advanced retrievals of multilayered cloud properties using multi-spectral measurements, *J. Geophys. Res.,* 110, D15S18, doi:10.1029/2004JD005101.

Korb, C.L., and Weng, C.Y.(1982). A theoretical study of a two-wavelength lidar technique for the measurement of atmospheric temperature profiles, *J. Appl. Meteorol.*, 21, 1346-1355, 1982.

Lawrence, R., Fralick, D., Harrah, S., Lin, B., Hu, Y., Hunt, P., Differential absorption microwave radar measurements for remote sensing of atmospheric pressure, Proceedings of the IEEE International Geoscience and Remote Sensing Symposium, July 2007.

Liebe, H.(1989). MPM--An atmospheric millimeter-wave propagation model. *Int. J. Infrared and Millimeter Waves*, 10, 631-650, 1989.

Liebe, H., Hufford, G., and Manabe, T. (1991). A model for complex permittivity of water at frequencies below 1 THz, *Int. J. Infrared Millimeter Waves*, 12, 659-675.

Lin, B., and Rossow, W.B.(1994). Observations of cloud liquid water path over oceans: Optical and microwave remote sensing methods, *J. Geophys. Res.*, 99, 20907-20927.

Lin, B., and Rossow, W. B. (1996). Seasonal variation of liquid and ice water path in non-precipitating clouds over oceans, *J. Clim., 9,* 2890-2902.

Lin, B., and Rossow, W. B. (1997). Precipitation water path and rainfall rate estimates over oceans using Special Sensor Microwave Imager and International Satellite Cloud Climatology Project data, *J. Geophys. Res.*, 102, 9359-9374.

Lin, B., Wielicki, B., Minnis, P., and Rossow, W.(1998a) Estimation of water cloud properties from satellite microwave, infrared and visible measurements in oceanic environments, 1. Microwave brightness temperature simulations, *J. Geophys. Res.*, *103*, 3873-3886.

Lin, B., Minnis, P., Wielicki, B., Doelling, D. R., Palikonda, R., Young, D. F., and Uttal, T. (1998b) Estimation of water cloud properties from satellite microwave, infrared and visible measurements in oceanic environment, 2. Results, *J. Geophys. Res.*,*103*, 3887-3905.

Lin, B. and Minnis, P. (2000). Temporal variations of land surface microwave emissivities over the ARM southern great plains site, *J. App. Meteor.*, 39, 1103-1116.

Lin, B., Minnis, P., Fan, A., Curry, J., and Gerber, H. (2001). Comparison of cloud liquid water paths derived from in situ and microwave radiometer data taken during the SHEBA/FIREACE, Geophys. Res. Letter, 28, 975-978.

Lin, B. and Hu, Y. (2005). Numerical Simulations of Radar Surface Air Pressure Measurements at O_2 Bands, *IEEE Geosci. and Remote Sensing Letter*, 2, 324-328.

Lin, B., Harrah, S., Neece, R. Lawrence, R., and Fralick, D. (2006). *The Feasibility of Radar-Based Remote Sensing of Barometric Pressure, Final Report*, NASA Earth Science Technology Office, August 10, 2006.

McClatchey, R., Fenn, R., Selby, J., Voltz, E., and Garing, J. (1972). *Optical properties of the atmospheric*, Air Force Cambridge Research Laboratories Environmental Research Paper AFCRL-72-0497, No. 411, 108pp.

Rosenkranz, P. (1998). Water vapor microwave continuum absorption: A comparison of measurements and models, *Radio Sci.*, 33, 919-928.

Ray, P. (1972). Broadband complex refractive indices of ice and water, *Appl. Opt.*, 11, 1836-1844.

Seemann, S. W., Li, J., Menzel, W. P., and Gumley, L. E. (2003). Operational retrieval of atmospheric temperature, moisture, and ozone from MODIS infrared radiances, *J. Appl. Meteorol.*, 42(8), 1072-1091.

Singer, S.F. (1968). Measurement of atmospheric surface pressure with a satellite–borne laser, Appl. Opp. 7, 1125-1127.

Wang, D–H., Droegemeier, K. K., Jahn, D., Xu, K. –M., Xue, M., and Zhang, J. (2001). NIDS-based intermittent diabatic assimilation and application to storm-scale numerical weather prediction. 14th Conf. On Numerical Weather Prediction and 18th Conf. On Weather and Forecasting, Amer. Meteor. Soc., Ft. Lauderdale, FL, 2001.

Wang, D. –H., and Minnis, P. (2003). *4D Data Reanalysis/Assimilation with Satellite, Radar and the Extensive Field Measurements*, CRYSTAL-FACE Science Team Meeting, Salt Lake City, UT, 24-28 Feb. 2003.

Wu, M.-L. (1985). Remote sensing of cloud top pressure using reflected Solar radiation in the Oxygen A-band, *J. Clim. Appl. Meteor.*, 24, 539-546.

Xiao, Q., Zou, X., and Wang, B. (2000). Initialization and simulation of a landfalling hurricane using a variational bogus data assimilation scheme, *Monthly Weather Review*, 128, 2252-2269.

Xue, M., Wang, D. –H., Gao, J. –D., Brewster, K., and Droegemeier, K. K. (2003). The Advanced Regional Prediction System (ARPS): storm-scale numerical weather prediction and assimilation. *Meteor. Atmos. Physics*, 82, 139-170.
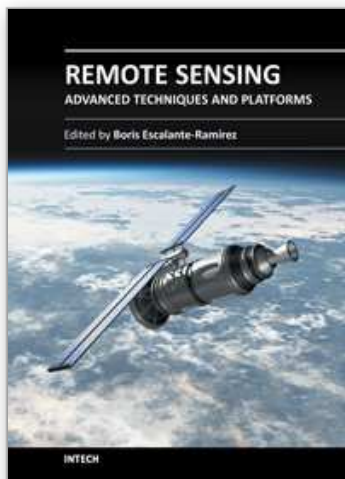
Remote Sensing - Advanced Techniques and Platforms

Edited by Dr. Boris Escalante

This dual conception of remote sensing brought us to the idea of preparing two different books; in addition to the first book which displays recent advances in remote sensing applications, this book is devoted to new techniques for data processing, sensors and platforms. We do not intend this book to cover all aspects of remote sensing techniques and platforms, since it would be an impossible task for a single volume. Instead, we have collected a number of high-quality, original and representative contributions in those areas.

How to reference

In order to correctly reference this scholarly work, feel free to copy and paste the following:

Roland Lawrence, Bin Lin, Steve Harrah and Qilong Min (2012). Differential Absorption Microwave Radar Measurements for Remote Sensing of Barometric Pressure, Remote Sensing - Advanced Techniques and Platforms, Dr. Boris Escalante (Ed.), ISBN: 978-953-51-0652-4, InTech, Available from: http://www.intechopen.com/books/remote-sensing-advanced-techniques-and-platforms/differential-absorption-microwave-radar-measurements-for-remote-sensing-of-barometric-pressure

INTECH
open science | open minds